ACS Photonics

Article

pubs.acs.org/journal/apchd5

Quenching, Plasmonic, and Radiative Decays in Nanogap Emitting Devices

Rémi Faggiani, Jianji Yang,*,# and Philippe Lalanne*

Laboratoire Photonique, Numérique et Nanosciences (LP2N), UMR 5298, CNRS-IOGS-University of Bordeaux, 33400 Talence, France

Supporting Information

ABSTRACT: By placing a quantum emitter in the mouths of nanogaps consisting of two metal nanoparticles nearly in contact, significant increases in emission rate are obtained. This mechanism is central in the design of modern plasmonic nanoantennas. However, due to the lack of general knowledge on the balance between the different decay rates in nanogaps (emission, quenching, and metal absorption), the design of light-emitting devices based on nanogaps is performed in a rather hazardous fashion; general intuitive recipes do not presently exist. With accurate and simple closed-form expressions for the quenching rate and the decay rate into gap plasmons, we provide a comprehensive analysis of nanogap light-emitting devices in the limit of small gap thickness. We disclose that the total decay rate in gap plasmons can largely overcome quenching for specifically selected metallic and insulator materials, regardless of the gap size. To confront these theoretical predictions, we provide a comprehensive numerical analysis of nanocube-type antennas in the limit of small gap thickness and further provide upper bounds for the photon-radiation efficiency.

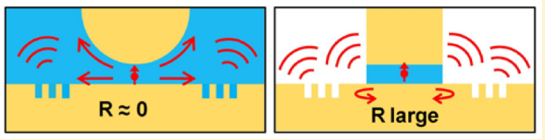

KEYWORDS: *optical nanoantennas, spontaneous emission, nanocavity, decay rates, modal formalism, quenching*

Dielectric nanogaps in metals have an unprecedented ability to concentrate light into deep-subwavelength volumes, which has propelled their use in a vast array of nanotechnologies and research topics.[1,2] For instance biological species can be manipulated at very low input powers by the field gradients at nanogaps,[3] photodetectors with sizes well below the diffraction limit may be implemented with very fast response time,[4] magnetic resonance supported by nanogap resonators can be utilized to realize negative-index metamaterials,[5,6] and feedgaps can be used to enhance the efficiency of high-harmonic nonlinear optical processes.[7] The strongly confined field also profoundly alters light emission of quantum emitters placed in the nanogap by increasing optical excitation rates, modifying radiative and nonradiative decay rates, and altering emission directionality, leading to a new generation of ultracompact nanoantenna architectures, such as bowties, spiral antennas, and phased-array antennas,[8] and to new applications for light-emitting devices,[9] broadband single-photon sources,[10−12] single-plasmon sources,[13,14] and spasers or low-threshold nanolasers.[15−17]

It is generally accepted that subwavelength architectures improve the exchange of optical energy with matter by strongly increasing spontaneous emission rates. As shown by numerical calculations and experimental measurements, it is also accepted that this enhancement can be achieved with relatively good efficiencies, ∼10−60% depending on the architecture. However, the precise physical mechanisms that drive the emission of quantum emitters placed very close to metal surfaces in tiny gaps are not well understood. In particular, it is unclear from the literature why good efficiencies are achieved despite the proximity to the metal, why quenching is not the dominant decay channel, what is the ultimate efficiency, and whether this limit is impacted by the gap thickness or other parameters.

To further explore how optical antennas may lead to new regimes of light−matter interactions, it is important to first understand the different channel decays at play when quantum emitters in 2D nanogaps emit light in the immediate vicinity of metal surfaces and then draw a relationship between this basic situation and more complex problems of light emission and coupling with nanogap antenna architectures.

This is exactly the approach that is adopted in the present work. First, we provide a comprehensive analysis of the decay rates of quantum emitters placed in 2D planar nanogaps. So far, this has been discussed only with scattered numerical calculations performed for specific gap thicknesses and metal dielectric constants.[11,18,19] In contrast, we derive a closed-form formula for the branching ratio between quenching and gap plasmon decays in the limit of small gap thicknesses and then clarify the key material and geometrical parameters that drive the ratio. Counterintuitively, we evidence that the key parameters are the material permittivities and not the gap thickness and that the gap plasmon decay surpasses the quenching decay for nanogaps fed with high-refractive-index materials and molecules polarized perpendicular to the gap interfaces.

Then we use the understanding gained from 2D planar structures to infer general recipes for designing efficient nanogap emitting devices. For that purpose, we model nanogap devices as gap-plasmon Fabry−Perot resonators and propose a

Received: July 31, 2015
Published: November 18, 2015

DOI: 10.1021/acsphotonics.5b00424
ACS Photonics 2015, 2, 1739−1744

phenomenological classification of nanogap antenna architectures, based on the trade-off between quenching, absorption, and free-space radiation rates, which may be monitored by controlling the gap-facet reflectance.

To set the classification against real structures, we analyze nanogap emitting devices formed by tiny nanocubes lying on metal surfaces. By scaling down the gap thickness and the cube dimensions to keep the resonance in the visible, distinct behaviors within the same architecture family are comprehensively reviewed. Our analysis corrects inaccurate numerical results of the recent literature[10,12] and definitely sets nanogaps with engineered facets as a very promising technological platform for light-emitting devices.

As a final point, we summarize the main results and provide a concluding discussion.

NONRADIATIVE DECAYS IN DIELECTRIC NANOGAPS

To start the analysis, let us consider the emission of a vertically polarized molecule (treated as an electric dipole) buried in the middle of a polymer layer of thickness $2d$ of a metal−insulator−metal (MIM) planar stack. Two channels are available for the decay. Either the molecule excites the gap plasmon modes of the planar stack or quenches by directly heating the metal. We denote by γ_{GSP} and γ_{quench} the corresponding normalized decay rates (all decay rates are normalized by the vacuum decay rate hereafter). Figure 1 summarizes the main trends for the decay rates for an emission wavelength at 650 nm and silver nanogaps. First we find that the direct decay in the metal, γ_{quench}, scales as d^{-3} as $d \to 0$. This scaling is understood from the local and static nature of quenching. Intuitively the quenching rate in a nanogap is expected to be ∼2 times larger than the quenching rate γ^{SI}_{quench} of the same vertical dipole on a *single interface* at the same separation distance d, and since $\gamma^{SI}_{quench} = (3/8\varepsilon_d(k_0d)^3)(\mathrm{Im}((\varepsilon_m - \varepsilon_d)/(\varepsilon_m + \varepsilon_d)))$ as $d \to 0$,[19] the cubic scaling is well anticipated. In fact, $\gamma_{quench} \approx 2\gamma^{SI}_{quench}$ holds for $d > 10$ nm only; as d decreases, we found empirically with numerical calculations performed at 650 nm that the quenching rate γ_{quench} is ∼3 times larger than γ^{SI}_{quench}.

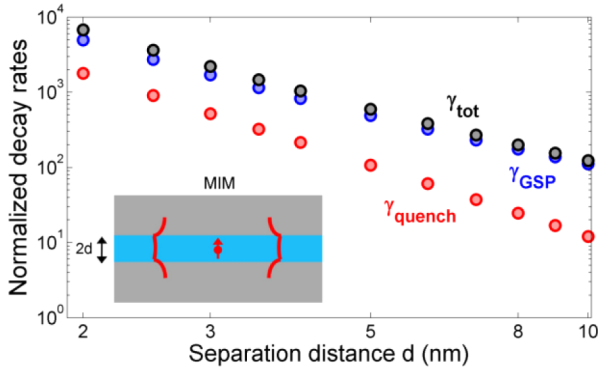

Figure 1. Competition between several decay channels for a vertical electric dipole emitting in the center of an Ag/polymer/Ag gap of width $2d$. The calculations are performed for an emission wavelength $\lambda_0 = 650$ nm. The refractive index of the polymer is $n = 1.4$, and the silver permittivity is $\varepsilon_{Ag} = -17 + 1.15i$.[20] The decay rates into all channels (γ_{tot}) and gap plasmons (γ_{GSP}) and the quenching rate (γ_{quench}) are shown with black, blue, and red circles, respectively. All the decay rates are normalized by the decay rate in the vacuum.

Importantly, we also find that the normalized decay rate into the gap plasmon modes of the planar stack also scales as the cube of the separation distance $2d$ between the metal films. What happens is the group velocity v_g of gap plasmons drastically decreases as d vanishes.[21] Slowdown results in a strong field enhancement, and the coupling to gap plasmons is boosted. Intuitively the fact that the plasmon decay rate and quenching have identical d^{-3} scaling can be understood by considering that as $d \to 0$, gap plasmons completely lose their photonic character. They are highly damped and become of the same nature as the quenching field. By using a complex continuation approach to calculate the Green tensor[22] and by assuming that the transverse electric and magnetic field components of the gap plasmon bear a flat profile within the gap, we have derived an analytical expression for γ_{GSP} for very small gap thickness, $\gamma_{GSP} \approx 12\pi\varepsilon_d/[(2k_0d)^3|\varepsilon_m|^2]$ (see Supporting Information for details), which evidences the inverse-cubic scaling.

Thus, we obtain an analytical expression for an important figure of merit of planar nanogaps with vanishing gap thicknesses, namely, the branching ratio F between gap-plasmon decay rates and quenching rates:

$$F \approx \frac{\gamma_{GSP}}{3\gamma^{SI}_{quench}} = \frac{2\varepsilon_d}{\mathrm{Im}(\varepsilon_m(\omega))}\left|\frac{\varepsilon_m(\omega)+\varepsilon_d}{\varepsilon_m(\omega)}\right|^2 \quad (1)$$

with ε_d and ε_m denoting the dielectric and metal permittivities. The formula carries important hints:

- First, the ratio is independent of d for $k_0d \to 0$, the first correction term being on the order of $O(k_0d)^2$, and takes a universal expression that depends only on the dielectric constants.
- Second, for good metals, $\varepsilon_d \ll |\varepsilon_m(\omega)|$, one should bury the quantum emitter in a high-index material to enhance the branching ratio in the near- and far-infrared spectral regions.
- Third, the ratio solely depends on the losses encountered in polarizing the material, i.e., on $\mathrm{Im}(\varepsilon_m(\omega))$, and not on the usual quality factor $-\mathrm{Re}(\varepsilon_m)/\mathrm{Im}(\varepsilon_m)$ of plasmonic materials, which gives an incontestable advantage to silver at visible frequencies, in comparison with gold or aluminum for instance.

Figure 2 shows typical branching ratios that can be obtained in the visible and near-infrared spectral regions with different metals and gap materials. The usefulness of the simple formula in eq 1 is reinforced by its ability to provide quantitative predictions, as evidenced with the comparison with fully vectorial computational data (shown with marks) obtained for planar nanogaps with small gap sizes ($d = 2$ nm). We emphasize that eq 1 is obtained in the asymptotic limit $k_0d \to 0$; as the gap thickness increases beyond the quasi-static approximation, the ratio F increases because quenching rapidly vanishes, and in this sense eq 1 actually sets a lower bound for the branching ratio. Overall, eq 1 represents a good compromise between simplicity or intuition and accuracy.

In the fully vectorial results shown in Figures 1 and 2, quenching rates are found as the difference between the total decay rates (calculated as the Poynting-vector flux on a close surface surrounding the emitter) and the decay rates into gap plasmon modes (calculated using an open-source software[23]). Details on the calculation technique are provided in the Supporting Information along with a verification that the

DOI: 10.1021/acsphotonics.5b00424
ACS Photonics 2015, 2, 1739−1744

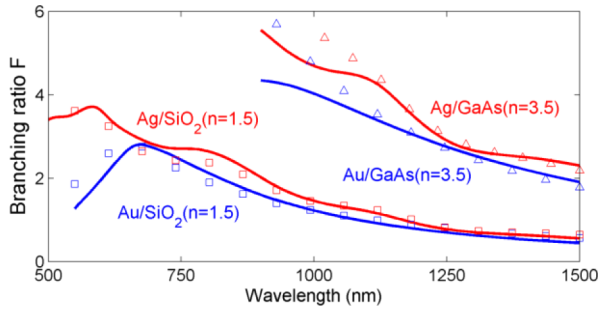

Figure 2. Branching ratios for nanogaps formed with various materials at visible and near-infrared frequencies. Fully vectorial calculations (for d = 2 nm) and analytical predictions from eq 1 are shown with markers and solid curves. Calculations made with Ag and Au are represented by red and blue colors, for dielectric (squares) and semiconductor (triangles) gap materials. Metal permittivities are taken from tabulated values.[20]

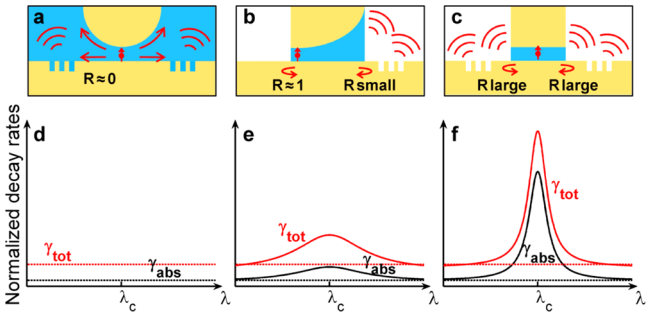

Figure 3. Classification of planar nanogap emitting devices with different degrees of decay rate enhancements. (a) Tapered devices with large photon-radiation efficiencies. Dipole emission is initially captured by gap plasmons and then adiabatically (low reflection $R \approx 0$) converted into photons. Grooves etched in the metal film help conversion of launched SPPs into free-space photons. (b) Nanoresonators with controlled facet reflectivities. (c) Nanoresonators with strong facet reflectivities. (d–f) Corresponding decay rates. (d) Due to the tapering, $\gamma_{tot} \approx \gamma_{GSP} + \gamma_{quench}$, where γ_{GSP} and γ_{quench} are the gap-plasmon and quenching decay rates obtained in a planar nanogap with a thickness equal to the mouth thickness. (e) The weak reflection in (b) results in a broadband rate enhancement with a large photon-radiation efficiency. (f) The strong reflection in (c) results in a narrowband Fabry–Perot resonance; γ_{tot} can be considerably boosted, but the nonradiative decay γ_{abs} due to cavity absorption lowers the photon-radiation efficiency.

indirect derivation of the quenched energy actually corresponds to the absorption in the near-field zone ($<0.02\lambda_0^2$) of the emitter.

CLASSIFICATION OF NANOGAP EMISSION DEVICES

Decay into plasmon modes is often considered as detrimental, just like quenching. However, it is of different nature since plasmons are coherent oscillations that may be transformed into free-space photons by scattering. This transformation is at the heart of nanogap-device design. Intuitively, gap devices can be thought of as Fabry–Perot nanoresonators with gap plasmon modes that bounce back and forth between two facets.[21,24,25] The nanoresonator modes can couple to different decay channels, i.e., to free-space photons and surface plasmon polaritons (SPPs) for nanoresonators surrounded by metal films, with normalized rates γ_{rad} and γ_{SP}, respectively. They also give rise to a new nonradiative decay, the mode absorption, with a decay rate γ_{abs}. Unlike quenching, which is intrinsically determined by proximity to metal, γ_{abs} is determined by the nanoantenna design and particularly the reflectivity R of the gap facets. Thus, from the sole knowledge acquired on the 2D planar structures and according to values of R that govern the resonance strength, we may distinguish three different nanogap-device categories, as illustrated in the classification of Figure 3.

Almost no reflectivity is implemented in tapered nanogaps formed for instance by curved and flat metal surfaces (Figure 3a) by adiabatically converting the slow gap-plasmons generated at the mouth[26−28] into free-space photons and SPPs launched on the flat metal surface surrounding the device. The SPPs can be further converted into photons with groove arrays for instance. Thus, the total decay rate is expected to be equal to $\gamma_{tot} \approx \gamma_{GSP} + \gamma_{quench}$, where γ_{GSP} and γ_{quench} are the gap-plasmon and quenching decay rates obtained in a planar nanogap with a thickness equal to the mouth thickness. For full SPP conversion into free-space photons, the photon-radiation efficiency is thus limited by quenching and is bounded by $F/(F + 1)$, a value that can be as large as 0.75 at an emission wavelength of 600 nm for Ag/polymer gaps (see Figure 2).

By contrast, for strong reflectivity favored by large impedance mismatch at the facet of tiny gaps[10,16] (see Figure 3c) the total decay rate is considerably boosted and quenching becomes completely negligible. However, the photon-radiation efficiency is limited by the absorption of gap plasmons in the tiny gap; it is expected to be much smaller than the value reached for adiabatically tapered antennas.

Figure 3b illustrates a promising class of nanogap antenna, with intermediate values of the facet reflectivity. Spontaneous-decay rates larger than γ_{GSP} are implemented, but the photon-radiation efficiency that is limited by quenching and absorption in the cavity may approach or even exceed the upper bound value of the $R \approx 0$ case.

NANOCUBE GEOMETRY

After this qualitative discussion, it is interesting to set the classification of Figure 3 against real nanogap emitting-device technologies. For that purpose, we consider devices formed by a tiny dielectric layer sandwiched between a metallic nanocube and a metallic substrate. This geometry that has been recently studied[10,12] is particularly suitable for exploring the three categories of the classification, since by scaling down the cube dimension, a whole family of gap emitting devices with distinct facet reflectivities can be straightforwardly designed and studied at the same resonant visible wavelength. But first let us begin by explaining how we calculate the photon-radiation efficiency and estimate the respective impact of quenching and gap-plasmon absorption. This is necessary because our results differ from those reported in refs 10 and 12 at least by a factor of 2 for the efficiency, and it is important to understand the reason.

We consider the same nanocube geometry as in ref 10 with a vertically polarized emitting dipole. The latter is placed in the middle of an 8 nm thick polymer gap at a cube corner, where maximum coupling with the resonance mode is achieved. Using COMSOL multiphysics, we first calculate the normalized total decay rate γ_{tot} by integrating the total power radiated around the source. Consistently with ref 10 at resonance γ_{tot} (black circles) is as large as 10^4, a value that represents a 10-fold enhancement, compared to the normalized gap-plasmon decay rate γ_{GSP} (cyan circles) obtained for a planar nanogap with the same materials and gap thickness.

DOI: 10.1021/acsphotonics.5b00424
ACS Photonics 2015, 2, 1739−1744

To provide a deeper insight, we also calculate the normalized decay rate γ_{mode} (i.e., the Purcell factor) into the fundamental magnetic-dipolar nanocube mode.[12] γ_{mode} is calculated by using a resonance-mode theory recently developed[29,30] for the analysis of plasmonic nanoresonators. Owing to the very small mode volume $V = (84\,000 + 8000i)$ nm^3 of the magnetic-dipolar mode, we find that 95% of the total decay is actually funneled into the resonance mode at resonance. The quenching rate γ_{quench} (red circles) is then calculated as $\gamma_{quench} = \gamma_{tot} - \gamma_{mode} - \gamma_{quad}$, where γ_{quad} represents a residual decay into a quadrupolar mode that resonates in the green.[31] Unlike intuitive statements in ref 10, our calculations indicate that quenching (red circles) is playing a negligible role, as its rate represents only ~2% of γ_{tot} at resonance. Then, using an open source code that computes the radiation diagrams of free-space and guided waves,[23] we calculate the normalized decays into free-space photons and SPPs launched around the nanocube, γ_{rad} and γ_{SP}, respectively. We find that ~60% of the mode energy is dissipated into heat, and the remaining 40% equally decays into free-space photons (20%) and SPPs (20%) that are launched on the flat metal interface surrounding the cube. This suggests the great potential of nanocubes for implementing plasmon sources. The present prediction $\gamma_{rad}/\gamma_{tot} \approx 20\%$ differs from the 50% photon-radiation efficiency calculated in refs 10 and 12 for the same geometrical parameters. We believe that the discrepancy is due to the fact that in refs 10 and 12 the photon-radiation efficiency is inferred from a direct computation of the Poynting-vector flux on a close surface surrounding the nanocube, without separating the respective contributions of the radiated photons and surface plasmons with a near-to-far-field transform.

Clearly, the nanocube antenna with a facet reflectivity of ~0.85, a value deduced from results reported in ref 21, belongs to the category of nanogap antennas with large facet reflectivities, i.e., case (c) in the classification of Figure 3.

We are now ready to study the nanocube performance for various thicknesses. For that, at every thickness, we adapt the cube size to maintain the magnetic-dipolar resonance at $\lambda_0 =$ 650 nm and repeat the previous modal analysis. The results for total decay rate γ_{tot} and the external efficiency $(\gamma_{rad} + \gamma_{SP})/\gamma_{tot}$ defined as the normalized decay into SPPs and photons are displayed in Figure 5a as a function of the gap thickness. The latter is shown to importantly impact the nanocube performance. As the thickness decreases, the facet reflectivity increases[21] and, accordingly, γ_{tot} strongly increases. However, the coupling to outgoing channels also decreases and the enhancement of the total decay rates is accompanied by a sudden drop of the external efficiency, from 80% for $d = 20$ nm to 15% for $d = 4$ nm.

For the sake of comparison, in Figure 5b, we display γ_{tot} and the external efficiency $(\gamma_{rad} + \gamma_{SP})/\gamma_{tot}$ (again, γ_{SP} denotes the decay to the SPPs on the flat metal surface, not gap plasmons) for a perfectly tapered antenna (case (a) of the classification in Figure 3). The predictions are obtained from planar nanogap calculations only, by assuming that $\gamma_{rad} + \gamma_{SP}$ is equal to the gap-plasmon decay rate γ_{GSP} in a planar nanogap with a thickness equal to the mouth thickness. This amounts to assuming that gap plasmons are fully converted by the tapering structure into SPPs and/or photons, and this provides an upper bound for the photon-radiation efficiency. As shown by a comparison between Figures 5a and b, smaller decay rates are achieved with the tapered antenna, but significantly larger external efficiencies are also obtained. Impressively, we predict that large efficiencies,

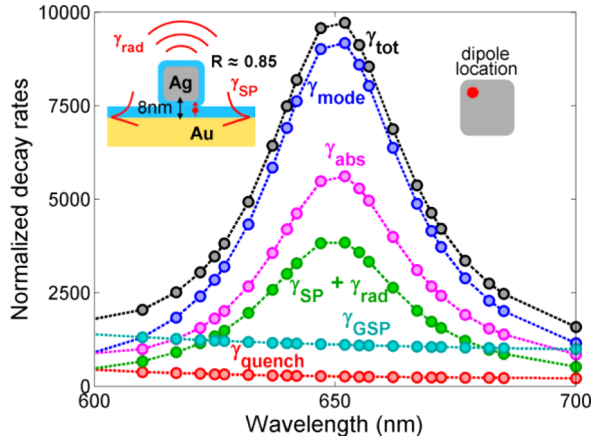

Figure 4. Decay channels of nanocube antennas. Calculated normalized decay rates of a vertical electric dipole at the corner (insets) of the antenna as a function of the wavelength. γ_{tot}, γ_{mode} (decay into the fundamental magnetic mode), γ_{abs} (antenna absorption), $\gamma_{rad} + \gamma_{SP}$ (sum of the radiative and SPP decay rates), and γ_{quench} are shown by black, blue, magenta, green, and red circles, respectively. γ_{GSP} (cyan) represents the decay into the gap plasmon of a planar nanogap of the same materials and gap thickness. Left inset: Cross-sectional view of the nanoantenna: a silver nanocube (side length 65 nm) with a 3 nm polymer coating ($n = 1.4$) is placed on a gold substrate covered by a 5 nm polymer (8 nm gap). The molecule is represented as a red arrow placed in the middle of the gap. Right inset: Top view of the cube showing the position of the dipole. The frequency-dependent permittivities, ε_{Ag} and ε_{Au}, of silver and gold are taken from tabulated data,[20] $\varepsilon_{Ag} = -17 + 1.15i$ and $\varepsilon_{Au} = -9.7 + 1.04i$ at $\lambda = 650$ nm.

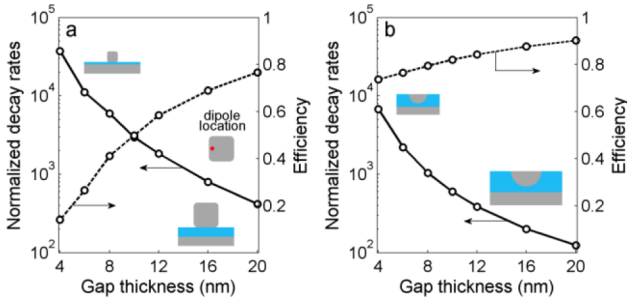

Figure 5. Patch versus tapered-nanogap antennas with polymer gaps. (a) Patch antennas. The calculations are performed for a vertical electric dipole located close to the center of the antenna facet (inset). The cube size varies with the gap thickness to maintain the resonance wavelength at 650 nm (side lengths are 47, 56, 65, 70, 75, 80, and 85 nm for gap thickness $d = 4$, 6, 8, 10, 12, 16, and 20 nm). (b) Perfectly tapered-nanogap antennas. The performances are predicted with planar-nanogap calculations by assuming perfect tapering of the gap-plasmons into SPPs and/or radiative photons. In (a) and (b), the normalized total decay rates γ_{tot} are shown with solid curves and the external efficiencies $(\gamma_{rad} + \gamma_{SP})/\gamma_{tot}$ with dashed curves.

>70%, with large normalized emission rates, ~10^3, are achieved for tiny nanogaps. Lastly, our simulations do not include additional loss mechanisms such as electron surface collisions,[9] but we use silver permittivity tabulated in ref 20, which exhibits a larger amount of nonradiative losses compared to other data sets. Regardless, even if doubts remain on the exact amount of losses in metal films/particles, our calculations open important perspectives for spontaneous light emission in general and definitely set nanogaps as a relevant technological platform. The future success of the platform will depend on fabrication

DOI: 10.1021/acsphotonics.5b00424
ACS Photonics 2015, 2, 1739−1744

and material issues and on our ability to engineer facet reflectivities adequately.

CONCLUDING DISCUSSION

Emitting photonic devices with quantum emitters embedded in nanogaps for operation at visible and near-infrared frequencies can provide large spontaneous emission rate enhancements and good photon-radiation efficiencies, because the decay into slow gap-plasmons is considerably boosted, and quenching is thus effectively overcome. This is particularly true for gaps with high-refractive-index insulators sandwiched between good metals, since the branching ratio $\propto \varepsilon_d/\mathrm{Im}(\varepsilon_m(\omega))$ between gap-plasmon decay rates and quenching rates reaches values as large as 80% for semiconductor gaps operated at near-infrared frequencies. The dominant character of plasmonic decays for small gaps has a direct impact on the design and performance of nanogap emitting devices. First, the high decay rates found in planar nanogaps can be harnessed to realize tapered antennas (Figure 3a) offering strong decay rate enhancements ($\approx 10^2$–10^3) and large photon-radiation efficiencies limited by the branching ratio between gap-plasmon decay rates and quenching rates; see eq 1. Second, even larger rate enhancements can be achieved in nanogap cavities (Figure 3c), which exhibit strong resonances owing to strong reflection of gap plasmons at the cavity facets. In return, the photon-radiation efficiency is significantly reduced by the cavity absorption, as indicated by the analysis of the state-of-the-art nanocube devices. Third, a better balance between decay rate enhancement and photon-radiation efficiency may be reached with nanogap antennas with engineered facet reflectivities (Figure 3b), for which a delicate engineering of the facets and a precise choice of the gap and metal materials may lead to acceleration decay rates greater than 10^3 with significant photon-radiation efficiency, ∼50%.

Certainly, the main strength of nanogap light-emitting devices is the capability to boost the spontaneous emission rate over a broad bandwidth with potentially easy electrical contacting. This might be useful for increasing quantum yield. However, the present analysis seems to indicate that it will be hard to achieve extremely high efficiencies (∼1), as required for some quantum-information protocols, and that the branching of eq 1 appears as a barrier for the photon-radiation efficiency, which will be hard to overcome.

ASSOCIATED CONTENT

Supporting Information

The Supporting Information is available free of charge on the ACS Publications website at DOI: 10.1021/acsphotonics.5b00424.

(1) Indirect calculation of quenching; (2) verification of the indirect quenching calculation and localized nature of the quenched fields; (3) asymptotic expression of γ_{GSP} for MIM stacks with vanishing gap thickness (PDF)

AUTHOR INFORMATION

Corresponding Authors

*E-mail: jianji.yang.photonique@gmail.com.
*E-mail: philippe.lalanne@institutoptique.fr.

Present Address

#Department of Electrical Engineering, Stanford University, Stanford, California 94305, United States.

Notes

The authors declare no competing financial interest.

ACKNOWLEDGMENTS

The authors thank Jean-Paul Hugonin for computational help. R.F. acknowledges financial support from the French "Direction Générale de l'Armement" (DGA).

REFERENCES

(1) Schuller, J. A.; Barnard, E. S.; Cai, W.; Jun, Y. C.; White, J. S.; Brongersma, M. l. Plasmonics for extreme light concentration and manipulation. *Nat. Mater.* **2010**, *9*, 193–204.

(2) Halas, N. J.; Lal, S.; Chang, W.-S.; Link, S.; Nordlander, P. Plasmons in strongly coupled metallic nanostructures. *Chem. Rev.* **2011**, *111*, 3913–3961.

(3) Roxworthy, B. J.; Ko, K. D.; Kumar, A.; Fung, K. H.; Chow, E. K. C.; Liu, G. L.; Fang, N. X.; Toussaint, K. C., Jr. Application of plasmonic bowtie nanoantenna arrays for optical trapping, stacking and sorting. *Nano Lett.* **2012**, *12*, 796–801.

(4) Ishi, T.; Fujikata, T.; Makita, K.; Baba, T.; Ohashi, K. Si nano-photodiode with a surface plasmon antenna. *Jpn. J. Appl. Phys.* **2005**, *44*, 364–366.

(5) Valentine, J.; Zhang, S.; Zentgraf, T.; Ulin-Avila, E.; Genov, D. A.; Bartal, G.; Zhang, X. Three-dimensional optical metamaterial with a negative refractive index. *Nature* **2008**, *455*, 376–379.

(6) Yang, J.; Sauvan, C.; Liu, H. T.; Lalanne, P. Theory of fishnet negative-index optical metamaterials. *Phys. Rev. Lett.* **2011**, *107*, 043903.

(7) Kim, S.; Jin, J.; Kim, Y.-J.; Park, I.-Y.; Kim, Y.; Kim, S.-W. High-harmonic generation by resonant plasmon field enhancement. *Nature* **2008**, *453*, 757–760.

(8) Agio, M. Optical antennas as nanoscale resonators. *Nanoscale* **2012**, *4*, 692–706.

(9) Eggleston, M. S.; Messer, K.; Zhang, L.; Yablonovitch, E.; Wu, M. C. Optical antenna enhanced spontaneous emission. *Proc. Natl. Acad. Sci. U. S. A.* **2015**, *112*, 1704–1709.

(10) Akselrod, G. M.; Argyropoulos, C.; Hoang, T. B.; Ciracì, C.; Fang, C.; Huang, J.; Smith, D. R.; Mikkelsen, M. H. Probing the mechanisms of large Purcell enhancement in plasmonic nanoantennas. *Nat. Photonics* **2014**, *8*, 835–840.

(11) Russell, K. J.; Liu, T.-L.; Cui, S.; Hu, E. L. Large spontaneous emission enhancement in plasmonic nanocavities. *Nat. Photonics* **2012**, *6*, 459–462.

(12) Rose, A.; Hoang, T. B.; McGuire, F.; Mock, J. J.; Ciracì, C.; Smith, D. R.; Mikkelsen, M. H. Control of radiative processes using tunable plasmonic nanopatch antennas. *Nano Lett.* **2014**, *14*, 4797–4802.

(13) Koenderink, A. F. Plasmon nanoparticle array waveguides for single photon and single plasmon sources. *Nano Lett.* **2009**, *9*, 4228–4233.

(14) Gan, C. H.; Hugonin, J.-P.; Lalanne, P. Proposal for compact solid-state III-V single plasmon sources. *Phys. Rev. X* **2012**, *2*, 021008.

(15) Khajavikhan, M.; Simic, A.; Katz, M.; Lee, J. H.; Slutsky, B.; Mizrahi, A.; Lomakin, V.; Fainman, Y. Thresholdless nanoscale coaxial lasers. *Nature* **2012**, *482*, 204–207.

(16) Oulton, R. F.; Sorger, V. J.; Zentgraf, T.; Ma, R.-M.; Gladden, C.; Dai, L.; Bartal, G.; Zhang, X. Plasmon lasers at deep subwavelength scale. *Nature* **2009**, *461*, 629–632.

(17) Lu, Y.-J.; Wang, C.-Y.; Kim, J.; Chen, H.-Y.; Lu, M.-Y.; Chen, Y.-C.; Chang, W.-H.; Chen, L.-J.; Stockman, M. I.; Shih, C.-K.; Gwo, S. All-color plasmonic nanolasers with ultralow thresholds: autotuning mechanism for single-mode lasing. *Nano Lett.* **2014**, *14*, 4381–4388.

(18) Jun, Y. C.; Kekatpure, R. D.; White, J. S.; Brongersma, M. L. Nonresonant enhancement of spontaneous emission in metal-dielectric-metal plasmon waveguide structures. *Phys. Rev. B: Condens. Matter Mater. Phys.* **2008**, *78*, 153111.

(19) Ford, G. W.; Weber, W. H. Electromagnetic interactions of molecules with metal surfaces. *Phys. Rep.* **1984**, *113*, 195–287.

DOI: 10.1021/acsphotonics.5b00424
ACS Photonics 2015, 2, 1739–1744

(20) Palik, E. D. *Handbook of Optical Constants*; Academic Press: San Diego, 1998.
(21) Yang, J.; Sauvan, C.; Jouanin, A.; Collin, S.; Pelouard, J.-L.; Lalanne, P. Ultrasmall metal-insulator-metal nanoresonators: impact of slow-wave effects on the quality factor. *Opt. Express* **2012**, *20*, 16880−16891.
(22) Collin, R. E. Hertzian dipole radiating over a lossy earth and sea: some early and late 20th-century controversies. *IEEE Antennas Propag. Mag.* **2004**, *46*, 64−79.
(23) Yang, J.; Hugonin, J.-P.; Lalanne, P. Near-to-far field transformations for radiative and guided waves. 2015, arXiv:1510.06344. arXiv.org e-Print archive. http://arxiv.org/abs/1510.06344 (accessed Oct 21, 2015).
(24) Miyazaki, H. T.; Kurokawa, Y. Squeezing visible light waves into a 3-nm-thick and 55-nm-long plasmon cavity. *Phys. Rev. Lett.* **2006**, *96*, 097401.
(25) Bozhevolnyi, S. I.; Søndergaard, T. General properties of slow-plasmon resonant nanostructures: nano-antennas and resonators. *Opt. Express* **2007**, *15*, 10869−10877.
(26) Fernández-Domínguez, A. I.; Maier, S. A.; Pendry, J. B. Collection and concentration of light by touching spheres: a transformation optics approach. *Phys. Rev. Lett.* **2010**, *105*, 266807.
(27) Yamamoto, N.; Ohtani, S.; García de Abajo, F. J. Gap and Mie plasmons in individual silver nanospheres near a silver surface. *Nano Lett.* **2011**, *11*, 91−95.
(28) Mubeen, S.; Zhang, S.; Kim, N.; Lee, S.; Krämer, S.; Xu, H.; Moskovits, M. Plasmonic properties of gold nanoparticles separated from gold mirror by an ultrathin oxide. *Nano Lett.* **2012**, *12*, 2088−2094.
(29) Sauvan, C.; Hugonin, J.-P.; Maksymov, I. S.; Lalanne, P. Theory of the spontaneous optical emission of nanosize photonic and plasmon resonators. *Phys. Rev. Lett.* **2013**, *110*, 237401.
(30) Bai, Q.; Perrin, M.; Sauvan, C.; Hugonin, J.-P.; Lalanne, P. Efficient and intuitive method for the analysis of light scattering by a resonant nanostructure. *Opt. Express* **2013**, *21*, 27371−27382.
(31) Britt Lassiter, J.; McGuire, F.; Mock, J. J.; Ciracì, C.; Hill, R. T.; Wiley, B. J.; Chilkoti, A.; Smith, D. R. Plasmonic waveguide modes of film-coupled metallic nanocubes. *Nano Lett.* **2013**, *13*, 5866−5872.

DOI: 10.1021/acsphotonics.5b00424
ACS Photonics 2015, 2, 1739−1744